Medical Engineering and Physics 73 (2019) 85–91

Contents lists available at ScienceDirect

Medical Engineering and Physics

journal homepage: www.elsevier.com/locate/medengphy

Technical note

Evaluation of predicted patellofemoral joint kinematics with a moving-axis joint model

C.M. Dzialo[a,b,*], P.H. Pedersen[c], K.K. Jensen[d], M. de Zee[e], M.S. Andersen[b]

[a] AnyBody Technology, A/S Niels Jernes Vej 10, DK 9220 Aalborg, Denmark
[b] Department of Materials and Production, Aalborg University, Fibigerstræde 16, DK-9220 Aalborg, Denmark
[c] Department of Orthopedic Surgery, Aalborg University Hospital, Hobrovej 18-22, DK-9000 Aalborg, Denmark
[d] Department of Radiology, Aalborg University Hospital, Hobrovej 18-22, DK-9000 Aalborg, Denmark
[e] Department of Health Science and Technology, Sport Sciences, Aalborg University, Fredrik Bajers Vej 7D, DK-9220 Aalborg, Denmark

ARTICLE INFO

Article history:
Received 20 December 2018
Revised 27 July 2019
Accepted 15 August 2019

Keywords:
Patellofemoral joint
Secondary joint kinematics
Magnetic resonance imaging
Musculoskeletal knee model
EOS imaging

ABSTRACT

The main objectives of this study were to expand the moving-axis joint model concept to the patellofemoral joint and evaluate the patellar motion against experimental patellofemoral kinematics. The experimental data was obtained through 2D-to-3D bone reconstruction of EOS images and segmented MRI data utilizing an iterative closest point optimization technique. Six knee model variations were developed using the AnyBody Modeling System and subject-specific bone geometries. These models consisted of various combinations of tibiofemoral (hinge, moving-axis, and interpolated) and patellofemoral (hinge and moving-axis) joint types. The newly introduced interpolated tibiofemoral joint is calibrated from the five EOS quasi-static lunge positions. The patellofemoral axis of the hinge model was defined by performing surface fits to the patellofemoral contact area; and the moving-axis model was defined based upon the position of the patellofemoral joint at 0° and 90° tibiofemoral-flexion. In between these angles, the patellofemoral axis moved linearly as a function of tibiofemoral-flexion, while outside these angles, the axis remained fixed. When using a moving-axis tibiofemoral joint, a hinge patellofemoral joint offers (-5.12 ± 1.23 mm, 5.81 ± 0.97 mm, $14.98 \pm 2.30°$, $-4.35 \pm 1.95°$) mean differences (compared to EOS) while a moving-axis patellofemoral model provides (-2.69 ± 1.04 mm, 1.13 ± 0.80 mm, $12.63 \pm 2.03°$, $1.74 \pm 1.46°$) in terms of lateral-shift, superior translation, patellofemoral-flexion, and patellar-rotation, respectively. Furthermore, the model predictive capabilities increased as a direct result of adding more calibrated positions to the tibiofemoral model (hinge-1, moving-axis-2, and interpolated-5). Overall, a novel subject-specific moving-axis patellofemoral model has been established; that produces realistic patellar motion and is computationally fast enough for clinical applications.

1. Introduction

The patellofemoral (PF) joint contains the body's largest sesamoid bone, the patella, nestled in the femoral trochlear groove. The patella acts as a lever arm to translate force from the quadriceps muscle across the tibiofemoral (TF) joint, while also serving as a bony shield to protect the tibiofemoral joint [1]. Dysfunction and mal-tracking often arise when the homeostasis of a joint is compromised [2–5], for example: increased patellar tilt [6,7], a more laterally positioned tibial tuberosity [8], abnormal "screw-home" rotation of the tibiofemoral joint [9], and hip muscle weakness [10] especially in the female population [11] may lead to anterior knee pain during activities of daily living. In addition, correlations exist between the patellofemoral morphology and resulting kinematics [7,12] so it is important that subject-specific morphology is captured when constructing musculoskeletal joint models.

Musculoskeletal modeling is a non-invasive computational tool used to better understand what occurs in the body internally as a result of external loads and movements. The patellofemoral joint is often excluded from pure kinematic models [13]; however when it is included, it is frequently modeled as a 1 degree-of-freedom hinge joint with an additional rigid patella tendon [14–22] which may not provide realistic joint kinematics. In hopes of achieving more realistic joint kinematics, researchers have included a 6 degrees-of-freedom patellofemoral joint utilizing multi-body contact models [17,23–31]. The main advantage of these models is that they can capture contact and ligaments forces; however, they may be too computationally slow for clinical applications.

* Corresponding author at: AnyBody Technology, A/S Niels Jernes Vej 10, DK 9220 Aalborg, Denmark.
E-mail address: cmd@anybodytech.com (C.M. Dzialo).

https://doi.org/10.1016/j.medengphy.2019.08.001
1350-4533/

The main objective of this study, therefore, was to establish a more computationally fast patellofemoral model capable of predicting subject-specific patellar motion when using motion capture input, while also avoiding error from skin artifact movement, for future use in the clinical setting. This model applies the concepts established in the moving-axis tibiofemoral joint model [32] to the patellofemoral joint. In a moving-axis joint applied to the knee (patellofemoral or tibiofemoral), the articulation is model such that the joint axis moves linearly back and forth between two known positions, as a function of tibiofemoral flexion. The proposed model was evaluated against the patellar positions extracted from a series of bi-planar EOS x-rays, which has an accurancy of 0.95 ± 0.55 mm [32].

2. Methods

2.1. Data collection

Preexisting imaging data [47], approved by the Scientific Ethical Committee for the Region of Nordjylland, was utilized in this study. This dataset consisted of lower limb Magnetic Resonance Image (MRI) acquisitions (T1W-LAVA-XV-IDEAL COR, 1.6 mm slice thickness, 0 mm gap thickness) of ten healthy male subjects (age 33 ± 10 years, body mass 79 ± 11 kg, height 1.82 ± 0.07 m) and five low dose radiation orthogonal x-rays (EOS^{TM}) of the loaded knee joint at roughly 0°, 20°, 45°, 60°, and 90° tibiofemoral-flexion during a quasi-static lunge.

2.2. Patella segmentation and registration

Bone surface geometries and contours of the patella were manually segmented from the lower limb MRIs and biplane EOS images, respectively, using Mimics Research 19.0 (Materialize, Leuven, Belgium). Custom MATLAB (The Mathworks Inc., Natick, MA, USA) code was used to manually transform the 3D bone geometry and its projected contours to roughly match the segmented biplanar contours. Then, an iterative closest point approach was employed to minimize the least-square difference between the contour sets. EOS reconstructions of the 3D patella positions and orientations for each set of EOS images were then read into the AnyBody Modeling System (AMS v 7.1, AnyBody Technology A/S, Denmark) to calculate translations and rotations of the patellofemoral joint.

2.3. Joint coordinate system (CS) and kinematic measures

For EOS data and all models, the patella anatomical CS origin was defined at the center of the outermost superior, inferior, medial, and lateral points. Each of these points were determined by first manually selecting the general location in 3-Matic Research 11.0 (Materialize, Leuven, Belgium), exporting this surface as a STL, and then taking an average of the STL cluster in MATLAB. The orientation was determined by (1) creating a temporary flexion axis running between the medial–lateral points, (2) defining the long axis (directed superiorly) between the superior–inferior points, (3) the anterior–posterior axis was defined as the cross product between (1) and (2), and finally the real medial–lateral axis was defined as the cross product between (2) and (3) [33–36]. We defined the patellofemoral joint in terms of a femoral and patella fixed-body axis with a perpendicular floating axis (Fig. 1), adapted from the ISB standards of the tibiofemoral joint [34,37,38]. The femoral anatomical axis was defined with the *y*-axis running from the center point between the two epicondyles to the hip joint center. The *z*-axis was defined orthogonal to the *y*-axis and pointing towards the lateral epicondyle. Finally, the *x*-axis is defined as the cross product between the *y*-axis and *z*-axis pointing anteriorly

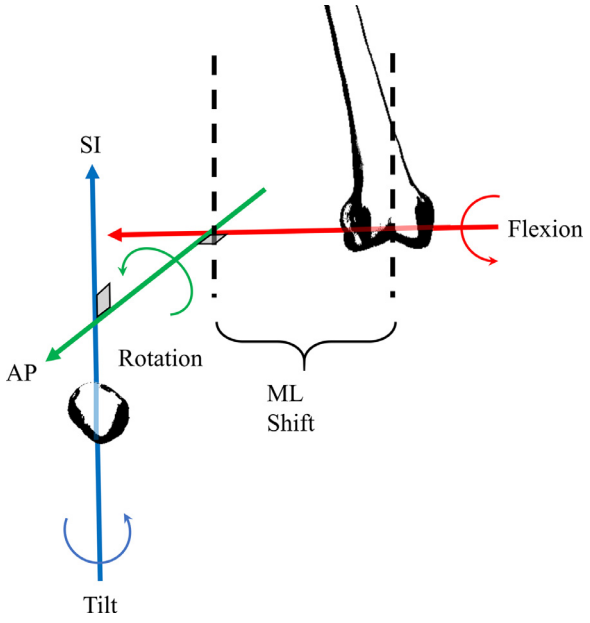

Fig. 1. Description of patellar motion: medial–lateral shift corresponds to the distance the patella origin moves along the fixed femoral axis (red), flexion is defined as how much the patella rotates about the fixed femoral axis (red), anterior–posterior translation corresponds to the distance the patella origin moves along the floating axis (green), rotation is the amount the patella rotates about the floating axis (green), superior–inferior translation corresponds to the distance traveled by the patella along the fixed patellar axis (blue), and Tilt is defined as the amount the patella rotates about the fixed patellar axis (blue). Image depicts directions of positive translations and rotations for right knee. (For interpretation of the references to colour in this figure legend, the reader is referred to the web version of this article).

[39–42,47]. The tibiofemoral joint was defined using ISB standards [37] and is discussed in detail in Dzialo et al. [47].

2.4. Knee model development

Six knee models were created using combinations of tibiofemoral and patellofemoral joint types (Supplementary Table 1). These joint types include: two previously established tibiofemoral joint models (hinge and moving-axis), one new tibiofemoral joint (Interpolation-INT), and two new patellofemoral joints (hinge and moving-axis). In each knee model, the patellar tendon is defined as a non-deformable element, connecting the patella to the tibia tuberosity.

2.4.1. Hinge

The tibiofemoral hinge joint axis was defined as a line running from the medial to lateral femoral epicondyles from the EOS_0 reconstruction pose [47]. To determine the patellofemoral hinge joint axis, we first applied a least-squares cylindrical fitting function using MATLAB to the medial and lateral surfaces of the femoral trochlear groove [43,44] to find the respective centers. The patellofemoral hinge joint axis was then defined by a line connecting these centers (Fig. 2(a)).

2.4.2. Moving-axis (MA)

The tibiofemoral MA joint model was taken directly from a previous study by Dzialo and co-workers [47]. The patellofemoral MA model was calibrated from the position and orientation of the patellofemoral joint in the 0° and 90° EOS reconstructions. We fit four cylinders to femoral trochlear groove surface selections (Fig. 2(b) and (c)), which were based on selections made by Bowes and co-workers [43,44] and discussed in the Hinge section above, based on where the patella contacts the femur when the

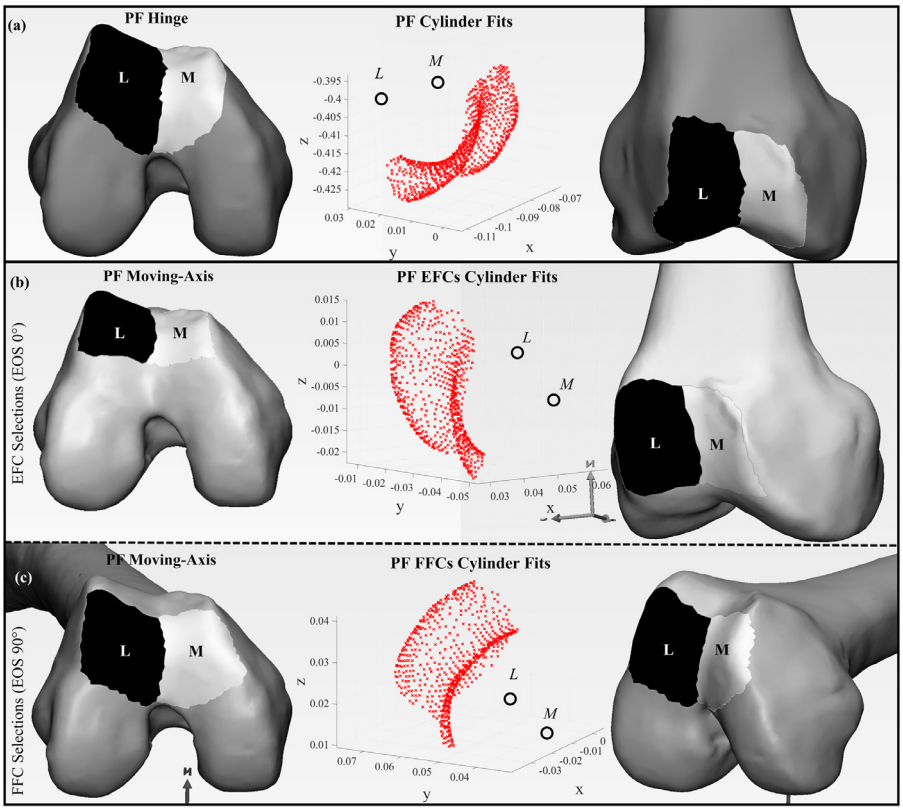

Fig. 2. Patellofemoral contact surface selections and corresponding analytical surface fits on (a) EOS_0 Femur for hinge joint definition (b) EOS_0 Femur for extension facet center definition (c) and EOS_90 femur for flexion facet center definition. (b–c) are combined to define the moving-axis patellofemoral joint.

tibiofemoral joint is in full extension (EOS-0), and in roughly 90° flexion (EOS-90). The facet centers from medial and lateral cylinder fits in extension (EFC) and flexion (FFC) were connected to define two axes (Fig. 2(b)–(c)). During hyperextension of the tibiofemoral joint, we assumed that the patellofemoral joint rotates about the EFC axis. For TF-flexion angles greater than the EOS 90° reconstruction, rotation occurs about the FFC axis. We assumed angles within these limits will move linearly as a function of TF-flexion between the patellofemoral EFC to FFC axes.

2.4.3. Interpolation (INT)

Due to the correlation between patellofemoral and tibiofemoral joint kinematics during weighted knee flexion, and the fact that the patellofemoral moving-axis is expressed as a function of the tibiofemoral flexion angle, the error present in the tibiofemoral joint may influence the model's predictability of the patellofemoral kinematics. This is especially the case in terms of PF-flexion, tilt, anterior–posterior (AP), and medial–lateral (ML) translations [45]. The Interpolation tibiofemoral model was simulated by applying a piecewise linear function, between the exact measured points from the tibiofemoral EOS reconstructions. With this, the only model error left would be within the patellofemoral model when comparing against the EOS experimental data.

2.5. Model evaluation and statistics

Patellofemoral kinematics were extracted from each EOS reconstruction (0°, 20°, 45°, 60°, and 90°). Corresponding model prediction results for each of the six model types were extracted at these TF-flexion angles. The 0° and 90° EOS reconstructions were not considered in the evaluation because they were used for model calibrations, eliminating any model predictive capabilities. The root mean square error (RMSE), mean differences with corresponding standard errors, Pearson's correlation coefficient (R), coefficient of determination (R^2), and adjusted R^2 were calculated for each of the six model predictions against the EOS experimental measures for each patellofemoral measure using SPSS version 25.0 (SPSS, Chicago, IL, USA). The absolute values of R were then categorized as weak, moderate, strong, or excellent prediction for $R \leq 0.35$, $0.35 < R \leq 0.67$, $0.67 < R \leq 0.90$, and $0.90 < R$, accordingly [46]. The data was tested for normality using Shapiro–Wilk tests. Eighteen one-way repeated measures ANOVAs (6 clinical measures at 3 lunge angles) were run with the necessary Greenhouse-Geisser corrections. Due to the multiple comparisons and a small sample size, post-hoc tests using Bonferroni adjustments ($\alpha = 0.05/18 = 0.002778$) were performed.

3. Results

Experimental and model subject means of each patellofemoral kinematic measure are depicted in Fig. 3, with standard deviations recorded in Supplementary Tables 2–8. Tables 1 and 2 display that the lowest RMSE and mean differences for medial–lateral shift, superior–inferior translation, flexion-extension, and patellar-rotation were achieved when utilizing a MA-PF joint, often decreasing with added known tibiofemoral positions (MA, INT). However, utilizing a MA-PF with any tibiofemoral joint type will result in underestimated tilt and AP translations. Additionally, the superior–inferior (SI) translation for high TF-flexion (60°) significantly overestimated the experimental data using a Hinge-PF for all tibiofemoral models. Although the AP and tilt remain best predicted by a Hinge-PF with MA-TF, the Int-TF with MA-PF de-

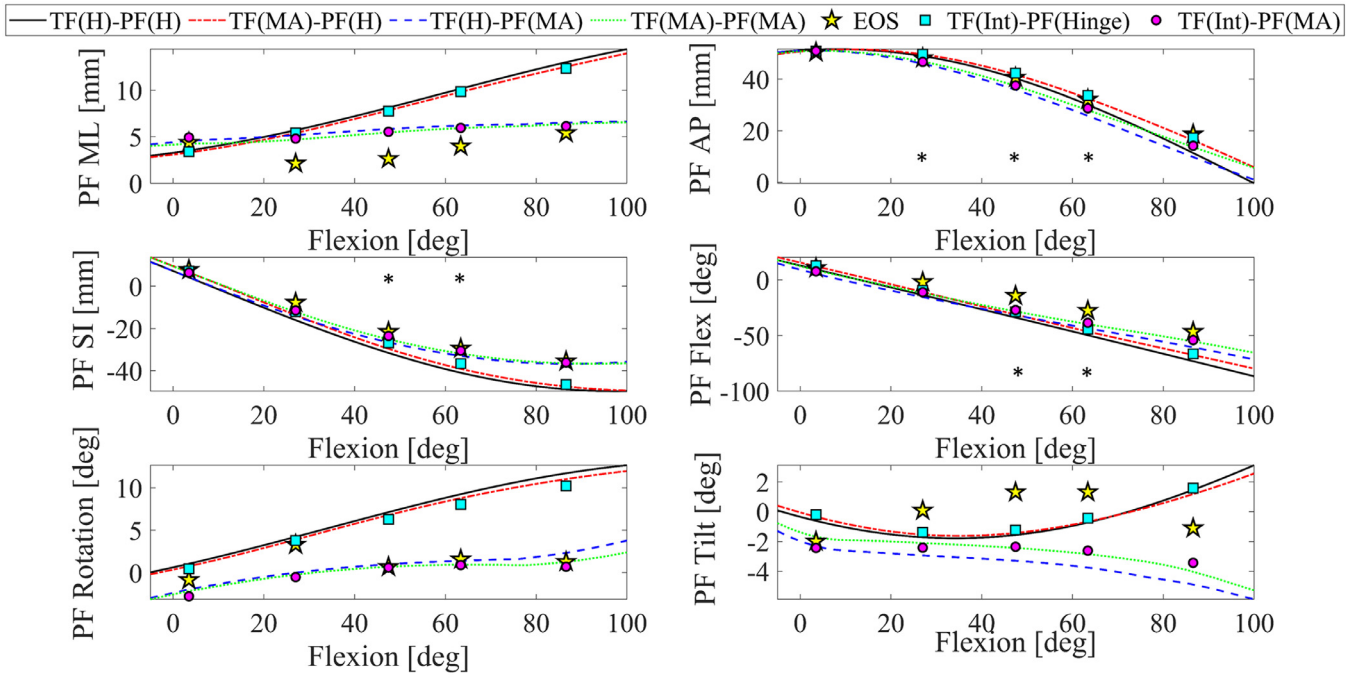

Fig. 3. Subject mean data ($n = 10$) of patellofemoral kinematic measures for the six model types and EOS data. Standard deviations are listed in a Supplementary Tables 1–7 to avoid clutter and make for a clear image. * designates that a significant differences exists between the experimental EOS data point and corresponding model data, please see Table 2 for specifics on which model(s).

Table 1
Root mean square error between experimental data (EOS) and various knee models for quasi-static lunge conditions with respect to femur reference frame for each clinical measure level for the given lunge conditions.

	Translations (mm)				Rotations (^{0})	
	ML	AP	SI	Flexion	Rotation	Tilt
EOS – hinge TF and PF						
20° flexion	4.54 ± 2.76	1.58 ± 1.33	7.44 ± 4.70	11.88 ± 7.55	4.26 ± 2.83	4.26 ± 5.57
45° flexion	6.13 ± 3.43	3.99 ± 2.40	6.72 ± 3.76	19.81 ± 6.35	6.96 ± 3.21	6.21 ± 4.20
60° flexion	6.70 ± 3.53	3.85 ± 2.80	9.30 ± 3.41	22.39 ± 7.38	8.75 ± 5.75	5.95 ± 4.08
Average	**5.79 ± 1.88**	**3.14 ± 1.31**	**7.82 ± 2.30**	**18.03 ± 4.11**	**6.66 ± 2.39**	**5.47 ± 2.69**
EOS – hinge TF: moving-axis PF						
20° flexion	3.77 ± 2.39	3.75 ± 1.67	5.50 ± 4.37	13.27 ± 10.66	5.45 ± 5.13	6.34 ± 6.13
45° flexion	3.91 ± 3.33	7.03 ± 1.89	2.80 ± 1.92	16.73 ± 7.42	3.94 ± 2.68	7.08 ± 7.27
60° flexion	2.65 ± 2.74	6.74 ± 2.76	1.81 ± 1.53	15.39 ± 7.54	4.03 ± 3.94	6.42 ± 6.07
Average	**3.45 ± 1.64**	**5.84 ± 1.25**	**3.37 ± 1.67**	**15.13 ± 5.01**	**4.47 ± 2.33**	**6.61 ± 3.76**
EOS – moving-axis TF: hinge PF						
20° flexion	4.32 ± 2.70	1.75 ± 1.07	5.29 ± 3.24	9.46 ± 6.41	4.16 ± 2.95	4.41 ± 5.47
45° flexion	5.91 ± 3.34	2.52 ± 1.39	4.66 ± 2.84	16.61 ± 7.17	6.86 ± 3.01	5.78 ± 4.01
60° flexion	6.47 ± 3.41	1.91 ± 1.35	7.46 ± 3.15	18.88 ± 8.23	8.72 ± 5.73	5.83 ± 3.99
Average	**5.57 ± 1.83**	**2.06 ± 0.74**	**5.81 ± 1.78**	**14.98 ± 4.22**	**6.58 ± 2.37**	**5.34 ± 2.62**
EOS –moving-axis: TF and PF						
20° flexion	3.47 ± 2.38	3.13 ± 1.90	4.03 ± 2.71	10.46 ± 8.00	5.54 ± 5.68	5.94 ± 5.71
45° flexion	3.64 ± 3.27	5.54 ± 1.44	1.82 ± 1.27	13.12 ± 6.00	4.17 ± 3.05	6.61 ± 6.45
60° flexion	2.36 ± 2.67	4.61 ± 1.99	1.23 ± 0.94	11.65 ± 4.50	3.94 ± 4.71	5.84 ± 5.28
Average	**3.16 ± 1.61**	**4.43 ± 1.03**	**2.36 ± 1.05**	**11.75 ± 3.66**	**4.55 ± 2.66**	**6.13 ± 3.37**
EOS – interpolated TF: hinge PF						
20° flexion	3.95 ± 2.51	2.00 ± 1.89	4.28 ± 2.48	7.79 ± 6.30	4.11 ± 3.27	4.59 ± 5.68
45° flexion	5.63 ± 3.06	1.82 ± 1.96	5.24 ± 2.57	14.49 ± 7.42	7.01 ± 3.10	5.53 ± 4.33
60° flexion	6.25 ± 3.29	2.01 ± 2.02	7.19 ± 3.21	16.75 ± 8.20	8.82 ± 5.59	5.73 ± 4.28
Average	**5.28 ± 1.72**	**1.94 ± 1.13**	**5.57 ± 1.60**	**13.01 ± 4.24**	**6.65 ± 2.39**	**5.28 ± 2.78**
EOS – interpolated TF: moving-axis PF						
20° flexion	3.29 ± 2.29	1.48 ± 1.41	3.83 ± 2.77	9.90 ± 8.11	5.38 ± 5.75	5.92 ± 5.29
45° flexion	3.49 ± 3.19	3.10 ± 1.74	2.41 ± 1.92	12.86 ± 6.22	4.65 ± 2.92	6.59 ± 6.29
60° flexion	2.35 ± 2.57	3.42 ± 2.23	1.52 ± 1.17	10.90 ± 4.90	4.08 ± 4.78	5.57 ± 5.10
Average	**3.04 ± 1.56**	**2.67 ± 1.05**	**2.59 ± 1.19**	**11.22 ± 3.78**	**4.70 ± 2.68**	**6.03 ± 3.22**

Table 2
Mean differences ± standard error between experimental data (EOS) and various knee models for quasi-static lunge conditions with respect to femur reference frame. Average (±SD) are calculated for each clinical measure. Symbol denotes that the clinical measure was statistically significantly different, appropriate Bonferroni adjustments were made for multiple comparisons, at *($\alpha = 0.05/18 = 0.002778$) level for the given lunge condition.

	Translations (mm)				Rotations (°)	
	ML	AP	SI	Flexion	Rotation	Tilt
EOS – hinge TF and PF						
20° flexion	−3.95 ± 1.15	1.04 ± 0.58	7.44 ± 1.49	11.88 ± 2.39	−1.02 ± 1.64	1.35 ± 2.22
45° flexion	−5.81 ± 1.26	3.86 ± 0.83	6.72 ± 1.19	19.81 ± 2.01*	−6.07 ± 1.53	2.01 ± 2.37
60° flexion	−6.46 ± 1.26	3.35 ± 1.09	9.3 ± 1.08*	22.39 ± 2.33*	−7.03 ± 2.51	1.55 ± 2.31
Average	**−5.41 ± 1.22**	**2.75 ± 0.83**	**7.82 ± 1.25**	**18.03 ± 2.24**	**−4.71 ± 1.89**	**1.64 ± 2.3**
EOS – hinge TF: moving-axis PF						
20° flexion	−3.29 ± 0.97	3.75 ± 0.53*	5.16 ± 1.52	13.01 ± 3.48	3.71 ± 2.10	3.47 ± 2.62
45° flexion	−3.36 ± 1.25	7.03 ± 0.60*	1.35 ± 1.02	16.73 ± 2.35*	0.03 ± 1.56	4.74 ± 2.89
60° flexion	−2.36 ± 0.95	6.74 ± 0.87*	1.40 ± 0.62	15.39 ± 2.39*	0.32 ± 1.83	5.17 ± 2.30
Average	**−3.01 ± 1.06**	**5.84 ± 0.67**	**2.63 ± 1.05**	**15.05 ± 2.74**	**1.35 ± 1.83**	**4.46 ± 2.61**
EOS – moving-axis TF: hinge PF						
20° flexion	−3.70 ± 1.13	0.59 ± 0.65	5.29 ± 1.03	9.46 ± 2.03	−0.75 ± 1.65	1.14 ± 2.24
45° flexion	−5.51 ± 1.27	2.2 ± 0.60	4.66 ± 0.90	16.61 ± 2.27*	−5.7 ± 1.59	1.91 ± 2.22
60° flexion	−6.14 ± 1.27	0.84 ± 0.71	7.46 ± 10.00*	18.88 ± 2.60*	−6.61 ± 2.62	1.48 ± 2.26
Average	**−5.12 ± 1.23**	**1.21 ± 0.65**	**5.81 ± 0.97**	**14.98 ± 2.30**	**−4.35 ± 1.95**	**1.51 ± 2.24**
EOS – moving-axis: TF and PF						
20° flexion	−2.91 ± 0.98	3.13 ± 0.60	3.26 ± 1.17	13.12 ± 2.77	3.97 ± 2.21	2.71 ± 2.52
45° flexion	−3.05 ± 1.23	5.54 ± 0.45*	−0.16 ± 0.73	13.12 ± 1.90*	0.43 ± 1.69	3.99 ± 2.69
60° flexion	−2.09 ± 0.92	4.61 ± 0.63*	0.28 ± 0.50	11.65 ± 1.42*	0.84 ± 0.50	4.41 ± 2.10
Average	**−2.69 ± 1.04**	**4.43 ± 0.56**	**1.13 ± 0.80**	**12.63 ± 2.03**	**1.74 ± 1.46**	**3.7 ± 2.44**
EOS – interpolated TF: hinge PF						
20° flexion	−3.29 ± 1.08	−1.5 ± 0.74	4.28 ± 0.79	7.52 ± 2.11	−0.49 ± 1.71	1.46 ± 2.31
45° flexion	−5.13 ± 1.24	−1.72 ± 0.65	5.24 ± 0.81*	14.49 ± 2.35	−5.59 ± 1.72	2.54 ± 2.13
60° flexion	−5.88 ± 1.26	−1.56 ± 0.77	7.19 ± 1.02*	16.75 ± 2.59*	−6.48 ± 2.67	1.76 ± 2.26
Average	−4.76 ± 1.19	−1.59 ± 0.72	5.57 ± 0.87	12.92 ± 2.35	−4.19 ± 2.03	1.92 ± 2.24
EOS – interpolated TF: moving-axis PF						
20° flexion	−2.67 ± 0.96	1.48 ± 0.45	3.68 ± 0.94	9.24 ± 2.83	3.82 ± 2.22	2.5 ± 2.45
45° flexion	−2.9 ± 1.2	3.1 ± 0.55	1.98 ± 0.76	12.86 ± 1.97*	0.08 ± 1.8	3.66 ± 2.7
60° flexion	−1.98 ± 0.91	3.42 ± 0.71	1.04 ± 0.52	10.9 ± 1.55*	0.67 ± 2.02	3.93 ± 2.08
Average	−2.52 ± 1.03	2.67 ± 0.57	2.23 ± 0.74	11 ± 2.11	1.52 ± 2.01	3.36 ± 2.41

Table 3
Model predictive capabilities: Pearson's correlation coefficient, coefficient of determination (R^2) and adjusted R^2 values calculated from model and experimental data (EOS) for quasi-static lunge angles (20°, 45°, 60°). R categorized as a weak (W) $r \leq 0.35$, moderate (M) $0.35 < r \leq 0.67$, strong (S) $0.67 < r \leq 0.90$, or excellent (E) $0.90 < r$ prediction.

	Model compared with EOS	*Translations*			*Rotations*		
		ML	AP	SI	Flexion	Rotation	Tilt
R	Hinge: TF and PF	0.30 (W)	0.96 (E)	0.95 (E)	0.91 (E)	0.39 (M)	0.39 (M)
	Hinge TF: MA PF	0.57 (M)	0.98 (E)	0.97 (E)	0.81 (S)	0.48 (M)	0.30 (W)
	MA TF: hinge PF	0.31 (W)	0.98 (E)	0.97 (E)	0.92 (E)	0.39 (M)	0.42 (M)
	MA: TF and PF	0.59 (M)	0.99 (E)	0.98 (E)	0.89 (S)	0.48 (M)	0.34 (W)
	Int. TF: hinge PF	0.62 (M)	0.99 (E)	0.98 (E)	0.88 (S)	0.47 (M)	0.36 (M)
	Int. TF: MA PF	0.36 (M)	0.98 (E)	0.98 (E)	0.92 (E)	0.41 (M)	0.42 (M)
R^2	Hinge: TF and PF	0.09	0.93	0.90	0.83	0.15	0.15
	Hinge TF: MA PF	0.32	0.95	0.93	0.66	0.23	0.09
	MA TF: hinge PF	0.10	0.96	0.94	0.85	0.15	0.17
	MA: TF and PF	0.35	0.98	0.96	0.80	0.23	0.11
	Int. TF: hinge PF	0.13	0.96	0.95	0.85	0.17	0.17
	Int. TF: MA PF	0.39	0.99	0.97	0.78	0.22	0.13
R^2_adj	Hinge: TF and PF	0.06	0.93	0.90	0.83	0.12	0.12
	Hinge TF: MA PF	0.30	0.95	0.93	0.65	0.20	0.06
	MA TF: hinge PF	0.07	0.96	0.94	0.85	0.12	0.14
	MA: TF and PF	0.33	0.98	0.95	0.79	0.21	0.08
	Int. TF: hinge PF	0.10	0.96	0.95	0.85	0.14	0.14
	Int. TF: MA PF	0.36	0.99	0.97	0.77	0.19	0.10

creases the mean differences in all measures besides SI. The commonly used hinge model presented the most significantly different patellofemoral measures when compared to the experimental EOS data especially in deep TF-flexion.

Overall, when using a MA-PF joint, the model predictive capabilities (R^2, R^2, and R^2_{adj}) increase for ML, AP, SI, and patellar-rotation measures (Table 3); and furthermore, increase when modeling the tibiofemoral with known positions (MA and INT models). Additionally, these measures all have strong to excellent prediction capabilities. However, a MA-PF joint does not necessarily improve the PF-flexion and tilt predictions, which both range in predictive capabilities from moderate to weak. PF-flexion is

best captured when modeling the tibiofemoral joint with known positions (MA and INT). In general, the ML-shift, patellar-rotation and tilt are not well predicted by the models, with adjusted R^2 values ranging from 0.06 to 0.38 (Table 3).

4. Discussion

This study presents a novel way of modeling the patellofemoral joint, utilizing MRI and EOS technology, and evaluates various models against in vivo kinematics extracted from consecutive quasi-static lunge positions. The moving-axis model is derived from subject-specific bone morphology and alignment. Being calibrated using two knee flexion positions (0° and 90°), the model captures the true tibiofemoral and patellofemoral kinematics at these poses and estimates what occurs in-between. Our results show that when changing a Hinge-PF to MA-PF joint provides more realistic patellar motion in terms of ML-shift, SI-translation, and patellar-rotation, when compared to experimental EOS. We found that AP translations are underestimated when using a MA-PF joint. This could partially be explained by the strong correlation between posterior patellar translation and posterior femoral translation [45] and the fact that our previously established tibiofemoral moving-axis and hinge models resulted in significantly underestimated AP translations for all lunge conditions [47]. Additionally, the overestimated patellofemoral flexion values for all models may be due to the constant patellar tendon length. In reality, the patellar tendon would elongate during 0 to 30 degree tibiofemoral flexion, and then stay relatively constant through 110 TF flexion [48]. Since we are holding this constant throughout the flexion cycle, there will be greater PF flexion in the models compared to that of the EOS reconstructions.

Kinematics of the patella during dynamic weight-bearing [49] and unloaded [50,51] activities may not be accurately predicted or represented from a passive supine position. Although bone geometries were from lower limb MRI, the initial model positions were set to the EOS-0 configuration (weight-bearing) to avoid these shortcomings. Patellofemoral kinematics can vary drastically between subjects and throughout the knee flexion cycle. If future aims include determining optimal patient treatments and or investigating injury progression it is important to consider subject-specific models that capture more than just one time point based off anatomical landmarks selections.

Applying a moving-axis model to the patellofemoral joint has its limitations. Patella instability normally occurs between 0° and 30° flexion. At this point, the patella may not be fully engaged with the trochlear groove, and or beyond this flexion may not track in smooth patella motion [10,52]. There is a chance that the patella was not sitting correctly in the trochlear groove during the EOS-0 scan. In these cases, a piecewise linear relationship may not result in correct patellar motion. Furthermore, the question of whether a linear relationship is appropriate for the MA-PF model is important to note; perhaps a polynomial relationship would fit better, but this would require fitting the model to more than two positions, like the INT-TF joint. In the future, evaluating other moving-axis relationships against dynamic in vivo data, at more extreme ROM, may provide a more comprehensive validation. Additionally, other computationally fast joint models should be considered such as a functional patellofemoral hinge axis. Although a functional PF hinge axis may have given better results than our cylinder fit hinge axis, we choose this for two main reasons: (1) it is know that for the tibiofemoral joint the cylinder fit hinge axis is a better anatomical surrogate compared to a trans-epicondylar hinge axis [53], we made the assumption that this would also hold true for the patellofemoral joint. (2) A functional patellofemoral hinge axis would require two poses of the patella relative to the femur, and many users may not have access to this kind data. While creating a hinge joint by fitting cylinders to scalable cadaver geometric data, similar to methods conducted in the Twente Lower Extremity Model [21], may be a more manageable option.

In conclusion, we have successfully applied the concept of a moving-axis model to the patellofemoral joint. The results show that a piecewise linear model can provide more accurate estimates of what is going on in the patellofemoral joint between two active TF-flexion positions when compared to the commonly used hinge joint. Most patellofemoral kinematics are best captured by using MA-PF with an INT-TF joint, followed by a MA-TF and then Hinge-TF with MA-PF. In order to bring musculoskeletal modeling of the patellofemoral joint to the clinical setting, the model needs capture more realistic joint kinematics (compared to the hinge) and be computationally fast (compared to the existing multi-body contact models). While applying a moving-axis joint partially accomplishes this, more investigation is needed to determine the best joint model for the clinical applications.

Declaration of Competing Interest

Mark de Zee is co-founder of the company AnyBody Technology A/S, owning the AnyBody Modeling System, which was used for the simulations. Mark de Zee is a minority shareholder on the company. Christine Dzialo, is now an Anybody Technology employee. However, during her participation in this project she was a PhD student under the supervision of Assoc. Prof. Michael Skipper Andersen and had nothing to do with Anybody Technology apart from using their software.

Acknowledgments

This study was performed under the KNEEMO Initial Training Network, funded by the European Union's Seventh Framework Program for research, technological development, and demonstration under Grant Agreement No. 607510 (www.kneemo.eu). This work was also supported by the Sapere Aude program of the Danish Council for Independent Research under grant no. DFF-4184-00018 to M. S. Andersen and the Innovation Fund Denmark under the Individualized Osteoarthritis Intervention project.

Ethical approval

This study was approved by the Scientific Ethical Committee for the Region of Nordjylland and informed consent was obtained prior to data collection.

J.nr.: 2016-000615

Supplementary materials

Supplementary material associated with this article can be found, in the online version, at doi:10.1016/j.medengphy.2019.08.001.

References

[1] Tecklenburg K, Dejour D, Hoser C, Fink C. Bony and cartilaginous anatomy of the patellofemoral joint. Knee Surg Sport Traumatol Arthrosc 2006;14:235–40. doi:10.1007/s00167-005-0683-0.

[2] Dye SF. Therapeutic implications of a tissue homeostasis approach to patellofemoral pain. Sports Med Arthrosc 2001;9:206–311. doi:10.1097/00132585-200110000-00008.

[3] Dye SF. Patellofemoral pain current concepts: an overview. Sports Med Arthrosc 2001;9:264–72. doi:10.1097/00132585-200110000-00002.

[4] Witvrouw E, Werner S, Mikkelsen C, Van Tiggelen D, Vanden Berghe L, Cerulli G. Clinical classification of patellofemoral pain syndrome: guidelines for non-operative treatment. Knee Surg Sport Traumatol Arthrosc 2005;13:122–30. doi:10.1007/s00167-004-0577-6.

[5] Crossley KM, Stefanik JJ, Selfe J, Collins NJ, Davis IS, Powers CM, et al. 2016 Patellofemoral pain consensus statement from the 4th International Patellofemoral pain research retreat, Manchester. part 1: terminology, definitions, clinical examination, natural history, patellofemoral osteoarthritis and patient-reported outcome m. Br J Sports Med 2016;50:839–43. doi:10.1136/bjsports-2016-096384.

[6] Wittstein JR, Bartlett EC, Easterbrook J, Byrd JC. Magnetic resonance imaging evaluation of patellofemoral malalignment. Arthroscopy 2006;22:643–9. doi:10.1016/j.arthro.2006.03.005.

[7] Lankhorst NE, Bierma-Zeinstra SMA, van Middelkoop M. Factors associated with patellofemoral pain syndrome: a systematic review. Br J Sports Med 2013;47:193–206. doi:10.1136/bjsports-2011-090369.

[8] Wittstein JR, O'Brien SD, Vinson EN, Garrett WE. MRI evaluation of anterior knee pain: predicting response to nonoperative treatment. Skeletal Radiol 2009;38:895–901. doi:10.1007/s00256-009-0698-6.

[9] Zhang LK, Wang XM, Niu YZ, Liu HX, Wang F. Relationship between patellar tracking and the "screw-home" mechanism of tibiofemoral joint. Orthop Surg 2016;8:490–5. doi:10.1111/os.12295.

[10] Waryasz GR, McDermott AY. Patellofemoral pain syndrome (PFPS): a systematic review of anatomy and potential risk factors. Dyn Med 2008;7:1–14. doi:10.1186/1476-5918-7-9.

[11] Prins MR, van der Wurff P. Females with patellofemoral pain syndrome have weak hip muscles: a systematic review. Aust J Physiother 2009;55:9–15. doi:10.1016/S0004-9514(09)70055-8.

[12] Sheehan FT, Derasari A, Fine KM, Brindle TJ, Alter KE. Q-angle and J-sign: indicative of maltracking subgroups in patellofemoral pain. Clin Orthop Relat Res 2010;468:266–75. doi:10.1007/s11999-009-0880-0.

[13] Moissenet F, Modenese L, Dumas R. Alterations of musculoskeletal models for a more accurate estimation of lower limb joint contact forces during normal gait: a systematic review. J Biomech 2017;63:8–20. doi:10.1016/j.jbiomech.2017.08.025.

[14] Sancisi N, Parenti-Castelli V. A new kinematic model of the passive motion of the knee inclusive of the patella. J Mech Robot 2011;3:041003. doi:10.1115/1.4004890.

[15] Lund ME, Andersen MS, de Zee M, Rasmussen J. Scaling of musculoskeletal models from static and dynamic trials. Int Biomech 2015:37–41. doi:10.1080/23335432.2014.993706.

[16] Habachi A El, Moissenet F, Duprey S, Cheze L, Dumas R. Global sensitivity analysis of the joint kinematics during gait to the parameters of a lower limb multi - body model. Med Biol Eng Comput 2015:655–67. doi:10.1007/s11517-015-1269-8.

[17] Marra MA, Vanheule V, Fluit R, Koopman BHFJM, Rasmussen J, Verdonschot N, et al. A subject-specific musculoskeletal modeling framework to predict in vivo mechanics of total knee arthroplasty. J Biomech Eng 2015;137:020904. doi:10.1115/1.4029258.

[18] Moissenet F, Chèze L, Dumas R. A 3D lower limb musculoskeletal model for simultaneous estimation of musculo-tendon, joint contact, ligament and bone forces during gait. J Biomech 2014;47:50–8. doi:10.1016/j.jbiomech.2013.10.015.

[19] Thelen DG, Won Choi K, Schmitz AM. Co-simulation of neuromuscular dynamics and knee mechanics during human walking. J Biomech Eng 2014;136:021033. doi:10.1115/1.4026358.

[20] Moissenet F, Chèze L, Dumas R. Influence of the level of muscular redundancy on the validity of a musculoskeletal model. J Biomech Eng 2016;138:021019. doi:10.1115/1.4032127.

[21] Carbone V, Fluit R, Pellikaan P,, ven der Krogt MM, Janssen D, Damsgaard M, et al. TLEM 2 .0 – a comprehensive musculoskeletal geometry dataset for subject-specific modeling of lower extremity. J Biomech 2015;48(5):734–41. doi:10.1016/j.jbiomech.2014.12.034.

[22] Brito da Luz S, Modenese L, Sancisi N, Mills PM, Kennedy B, Beck BR, et al. Feasibility of using MRIs to create subject-specific parallel-mechanism joint models. J Biomech 2017;53:45–55. doi:10.1016/j.jbiomech.2016.12.018.

[23] Marra MA, Strzelczak M, Heesterbeek PJC, van de Groes SAW, Janssen DW, Koopman BFJM, et al. Anterior referencing of tibial slope in total knee arthroplasty considerably influences knee kinematics: a musculoskeletal simulation study. Knee Surg Sport Traumatol Arthrosc 2017:1–9. doi:10.1007/s00167-017-4561-3.

[24] Halonen KS, Dzialo CM, Mannisi M, Venäläinen MS, de Zee M, Andersen MS. Workflow assessing the effect of gait alterations on stresses in the medial tibial cartilage – combined musculoskeletal modelling and finite element analysis. Sci Rep 2017;7:17396. doi:10.1038/s41598-017-17228-x.

[25] Smith CR, Vignos MF, Lenhart RL, Kaiser J. The influence of component alignment and ligament properties on tibiofemoral contact forces in total knee replacement. J Biomech Eng 2017;138:021017. doi:10.1115/1.4032464.

[26] Guess TM, Stylianou AP, Kia M. Concurrent prediction of muscle and tibiofemoral contact forces during treadmill gait. J Biomech Eng 2014;136:021032 1–9. doi:10.1115/1.4026359.

[27] Hast MW, Piazza SJ. Dual-joint modeling for estimation of total knee replacement contact forces during locomotion. J Biomech Eng 2013;135:021013. doi:10.1115/1.4023320.

[28] Lenhart RL, Kaiser J, Smith CR, Thelen DG. Prediction and validation of load-dependent behavior of the tibiofemoral and patellofemoral joints during movement. Ann Biomed Eng 2015;43:2675–85.

[29] Smith CR, Lenhart BSRL, Thelen DG, Kaiser J, Vignos MF. Influence of ligament properties on tibiofemoral mechanics in walking. J Knee Surg Knee Surg 2016;29:99–106.

[30] Walter JP, Kinney AL, Banks S a, D'Lima DD, Besier TF, Lloyd DG, et al. Muscle synergies may improve optimization prediction of knee contact forces during walking. J Biomech Eng 2014;136:021031. doi:10.1115/1.4026428.

[31] Serrancolí G, Kinney AL, Fregly BJ, Font-Llagunes JM. Neuromusculoskeletal model calibration significantly affects predicted knee contact forces for walking. J Biomech Eng 2016;138:081001. doi:10.1115/1.4033673.

[32] Pedersen D, Vanheule V, Wirix-Speetjens R, Taylan O, Delport HP, Scheys L, et al. A novel non-invasive method for measuring knee joint laxity in 6-DOF: in vitro proof-of-concept and validation. J Biomech 2018. doi:10.1016/j.jbiomech.2018.10.016.

[33] Goh JC, Lee PY, Bose K, Goh JC. A cadaver study of the function of the oblique part of vastus medialis. J Bone Jt Surgery Br Vol 1995;77:225–31. doi:10.2106/00004623-199502000-00008.

[34] Bull AMJ, Katchburian MV, Shih YF, Amis AA. Standardisation of the description of patellofemoral motion and comparison between different techniques. knee surgery. Sport Traumatol Arthrosc 2002;10:184–93. doi:10.1007/s00167-001-0276-5.

[35] Kedgley AE, McWalter EJ, Wilson DR. The effect of coordinate system variation on in vivo patellofemoral kinematic measures. Knee 2015;22:88–94. doi:10.1016/j.knee.2014.11.006.

[36] Amis AA, Senavongse W, Bull AMJ. Patellofemoral kinematics during knee flexion–extension: an in vitro study. J Orthop Res 2006:2201–11.

[37] Grood ES, Suntay W. A joint coordinate system for the clinical description of three-dimensional motions: application to the knee. J Biomech Enginering 1983;105:136–44.

[38] Hefzy MS, Jackson WT, Saddemi SR, Hsieh YF. Effects of tibial rotations on patellar tracking and patello-femoral contact areas. J Biomed Eng 1992;14:329–43. doi:10.1016/0141-5425(92)90008-9.

[39] Pennock GR, Clark KJ. An anatomy-based coordinate system for the description of the kinematic displacements in the human knee. J Biomech 1990;23:1209–18. doi:10.1016/0021-9290(90)90378-G.

[40] Suzuki T, Hosseini A, Li J-S, Gill TJ, Li G. In vivo patellar tracking and patellofemoral cartilage contacts during dynamic stair ascending Takashi. J Biomech 2012;45:2432–7. doi:10.1016/j.jbiomech.2012.06.034.

[41] Churchill DL, Incavo SJ, Johnson CC, Beynnon BD. The transepicondylar axis approximates the optimal flexion axis of the knee. Clin Orthop Relat Res 1998:111–18.

[42] Most E, Axe J, Rubash H, Li G. Sensitivity of the knee joint kinematics calculation to selection of flexion axes. J Biomech 2004;37:1743–8. doi:10.1016/j.jbiomech.2004.01.025.

[43] Bowes MA, Vincent GR, Wolstenholme CB, Conaghan PG. A novel method for bone area measurement provides new insights into osteoarthritis and its progression. Ann Rheum Dis 2015;74:519–25. doi:10.1136/annrheumdis-2013-204052.

[44] Drew BT, Bowes MA, Redmond AC, Dube B, Kingsbury SR, Conaghan PG. Patellofemoral morphology is not related to pain using three-dimensional quantitative analysis in an older population: data from the osteoarthritis initiative. Rheumatology 2017:2135–44. doi:10.1093/rheumatology/kex329.

[45] Li G, Papannagari R, Nha KW, Defrate LE, Gill TJ, Rubash HE. The coupled motion of the femur and patella during in vivo weightbearing knee flexion. J Biomech Eng 2007;129:937–43. doi:10.1115/1.2803267.

[46] Taylor R. Interpretation of the correlation coefficient: a basic review. J Diagnostic Med Sonogr 1990;1:35–9.

[47] Dzialo CM, Pedersen PH, Simonsen CW, Jensen KK, de Zee M, Andersen MS. Development and validation of a subject-specific moving-axis tibiofemoral joint model using mri and eos imaging during a quasi-static lunge. J Biomech 2018;72:71–80. doi:10.1016/J.JBIOMECH.2018.02.032.

[48] Defrate LE, Nha KW, Papannagari R, Moses JM, Thomas J, Li G. The biomechanical function of the patellar tendon during *in-vivo* weight-bearing flexion. J Biomech 2008;40:1716–22.

[49] Draper CE, Besier TF, Fredericson M, Santos JM, Beaupre GS, Delp SL, et al. Differences in patellofemoral kinematics between weight-bearing and non-weight-bearing conditions in patients with patellofemoral pain. J Orthop Res 2011;29:312–17. doi:10.1002/jor.21253.

[50] Freedman BR, Sheehan FT. Predicting three-dimensional patellofemoral kinematics from static imaging-based alignment measures. J Orthop Res 2015;31:441–7. doi:10.1002/jor.22246.

[51] D'Entremont AG, Nordmeyer-Massner JA, Bos C, Wilson DR, Pruessmann KP. Do dynamic-based mr knee kinematics methods produce the same results as static methods? Magn Reson Med 2013;69:1634–44. doi:10.1002/mrm.24425.

[52] Amis A. Current concept on anatomy and biomechanics of patellar stability. Sport Med Arthrosc Rev 2007;15:48–56.

[53] Yin L, Chen K, Guo L, Cheng L, Wang F, Yang L. Identifying the functional flexion-extension axis of the knee: an in-vivo kinematics study. PLoS ONE 2015;10:1–11. doi:10.1371/journal.pone.0128877.